UNIVERSITY OF CALIFORNIA SAN DIEGO

Dissecting the mechanistic basis of nuclear migration during stomatal formation in *Arabidopsis thaliana*

A Thesis submitted in partial satisfaction of the requirements
for the degree Master of Science

in

Biology

by

Lili Follett

Committee in charge:

Professor Andrew Muroyama, Chair
Professor Alexandra Jazz Dickinson
Professor Mark Estelle

2024

The Thesis of Lili Follett is approved, and it is acceptable in quality and form for publication on microfilm and electronically.

University of California San Diego

2024

TABLE OF CONTENTS

LIST OF FIGURES

LIST OF TABLES

LIST OF ABBREVIATIONS

ACD	Asymmetric Cell Division
dpg	Days post-germination
CRWN	CROWDED NUCLEI
SLGC	Stomatal Lineage Guard Cell
KRN2/OsKRN2.	KERNEL ROW NUMBER 2
WASp	Wiskott-Aldrich Syndrome Protein
WIP	WASp INTERACTING PROTEIN
Dsh	DISHEVELLED
MMC	Meristemoid mother cell
bHLH	Basic helix-loop-helix
SPCH	SPEECHLESS
BASL	BREAKING OF ASYMMETRY IN THE STOMATAL LINEAGE
BRXf	BREVIS RADIX family
GSK3	GLYCOGEN SYNTHASE KINASE3
SUN	Sad1/UNC-84
MS	Murashige and Skoog
PI	Propidium iodide (PI)
TMM	TOO MANY MOUTHS

ACKNOWLEDGEMENTS

I would like to thank Andrew Muroyama for his expertise, guidance, and support throughout the process of research and as the chair of my committee. His support has been invaluable throughout this process.

In addition, I would like to thank Kensington Hartman for her help during the imaging process and for her support through all my procedures in lab.

Thank you to Gabriel Angres for his support and assistance throughout the process of writing this thesis.

I would also like to thank Nathaniel Takatsuno for his support and for teaching me how to carry out many of the protocols needed for this research.

Thank you to Tyler Castro for his assistance in plating seeds and genotyping.

ABSTRACT OF THE THESIS

Dissecting the mechanistic basis of nuclear migration during stomatal formation in *Arabidopsis thaliana*

by

Lili Follett

Master of Science in Biology

University of California San Diego, 2024

Professor Andrew Muroyama, Chair

Stem cell differentiation is key to plant development, which utilizes asymmetric cell divisions (ACD) to maintain stem cells, promote growth, and encourage cell diversity. Previous work in *Arabidopsis thaliana* elucidated some pathways controlling stem cell dynamics during morphogenesis. In the leaf epidermis, pre-mitotic, oriented nuclear migrations in meristemoids, a transient stem cell in *Arabidopsis thaliana,* allow creation of daughter cells with differing sizes,

fates, and placements. Pre-division, the nucleus uses microtubules to migrate away from a polarity crescent that controls division orientation. Post-division, it is known that the nucleus orients towards the polarity crescent using F-actin, but precise mechanisms, including relevant nucleators, are unknown. Additionally, while behavior of the nucleus during ACDs in meristemoids has been characterized, cytoskeletal regulators linking the nucleus to F-actin remain unknown.

Time-lapse imaging of *Arabidopsis* seedlings treated with an F-actin Arp2/3 complex inhibitor (CK-666) and a control compound (CK-689), revealed that Arp2/3 complex-mediated F-actin controls nuclear migration post-division. Novel regulators of nuclear migration were found by phenotypic characterization of stomatal formation in loss-of-function mutants in protein components linking the cytoskeleton to the nuclear envelope. We found three candidate proteins (CRWN1, CRWN3, and SINE1) decreased stomatal density, while one (SUN1) increased stomatal density. This suggests ACD frequency is altered in these mutants and identifies new factors to probe in future studies.

These candidate proteins, SUN1, CRWN1, CRWN3, and SINE1, may control nuclear migration in *Arabidopsis thaliana*, alongside Arp2/3 complex-mediated F-actin. Determining mechanisms behind nuclear migration gives insight into how organelle positioning controls ACDs and stomatal development.

CHAPTER 1: INTRODUCTION

Stem Cells Create Tissues During Development

Stem cells are specialized cells in an organism that can generate cells of diverse fates while also regenerating their own population. Because these undifferentiated cells are essential for organismal development and homeostasis, significant research effort has focused on understanding stem cell dynamics in animals and how stem cells can be utilized for therapeutic applications.

Plants also contain stem cell populations, which reside in the shoot, root, and cambium meristems. Shoot and root apical meristems aid in longitudinal plant growth and are maintained in stem cell niches, which are specialized microenvironments that maintain proper stem cell function and control long-term growth. Shoot apical meristems also act as the source for cells required to make a plant's flowers, stem, and leaves, whereas the root apical meristem is required for continual root growth. Cambium meristems primarily mediate secondary growth, such as creating vascular tissue, forming the shape of internodes, and thickening the stem (Laux 2003; Jiang & Feldman 2005; Poliwoda et al. 2022). Plant meristems are maintained throughout the life of the plant almost indefinitely and are able to generate new cells as needed (Zhou et al. 2019; Pardal and Heidstra 2021).

In humans, stem cell dysregulation can give rise to multiple diseases, such as cancer (Lytle et al. 2018). However, at the same time, human stem cells have become clinically important and are also used therapeutically to treat once deadly or disabling diseases and injuries, such as diabetes, liver failure, spinal cord injuries, and Parkinson's disease (Volarevic et al. 2011). Because stem cells affect growth and development, there is hope that stem cells in plants could similarly be used for agricultural applications, such as to increase

hardiness or crop yield. For example, the stem cell regulator gene, *KERNEL ROW NUMBER 2* (KRN2/OsKRN2) in rice and maize, is known to improve crop yield (Chen et al. 2022). Therefore, understanding the regulation of stem cells in plants holds significant promise for future agricultural applications.

Asymmetric Cell Division in Animals

Asymmetric divisions are vital to stem cell maintenance and cell differentiation in both plants and animals. Asymmetric divisions occur when a stem cell divides during mitosis to create two daughter cells of differing fates. Typically, one daughter cell remains a stem cell while the other goes on towards differentiation. While defined by their ability to generate daughter cells of different identities, ACDs can also generate daughter cells of different sizes. In animals, defects in asymmetric cell division can lead to incorrect cell fates, tissue defects, and cancer (Gillies & Cabernard 2011; Liu et al. 2018; Knoblich 2010; Neumüller & Knoblich 2009).

Because ACDs are responsible for maintaining a stem cell pool (typically in a niche) and also generating differentiating daughters, the orientation of most ACDs is tightly controlled. In animals, division orientation is primarily based on the orientation of the mitotic spindle, which can be regulated by intrinsic cues, such as cell polarity, and/or extrinsic factors, such as signaling molecules.

Cell polarity, defined here as intrinsic asymmetry driven by biased protein localization to one side of the cell, allows a cell to divide its components unequally during divisions to create daughter cells with differing fates. To create cell polarity, a polarized protein complex, or polarity crescent, typically forms at a specific site on the plasma membrane. In the most well-studied case (from *S. cerevisiae*) small GTPases such as Rho and Cdc42p polarize and

begin the process of localized F-actin assembly. Depending on the cellular context, this can involve recruitment and activation of the Arp2/3 actin complex, profilin, myosins, WASp/WIP, and formins. The polar domain can also serve as a local site for vesicle delivery via myosins, SNAREs, Sec4p and exocyst and microtubule assembly (Kar9p/Bim1p and Tea1p/Tip1p/Mal3p) (Nelson 2003). Changes to the cell's polarity or polarity crescent lead to a change in the division orientation as well. For example, in zebrafish embryos, orientation of the divisions in epiblast cells are dependent on the Dishevelled (Dsh) gene, which controls the length of the cell's polarity crescent (Gibieža and Petrikaitė 2021). When size or orientation of a cell's polarity crescent is altered, division dynamics are also altered, as divison orientation is mediated through positioning of the polarity crescent and mitotic spindle.

The positioning of the mitotic spindle is also a crucial determinant of proper division orientation, as it sets the position of the division axis and the cleavage furrow. In the canonical case, cortical dynein is localized to one side of the cell by the polarity domain, allowing it to exert a pulling force on astral microtubules that emanate from the spindle poles (Tame et al. 2014; Jan & Jan 2000; Bergstralh et al. 2017). This spindle orientation mechanism intersects with polarity during ACD through a highly conserved mechanism that was first described in the one-cell C. elegans zygote (Gönczy et al. 1999; Bouvrais et al. 2021). When the dynein heavy chain was depleted in C. elegans, it was found that while the centrosome was able to be separated, the positioning of the mitotic spindle was defective. This indicates that pulling forces on astral microtubules, which position the mitotic spindle, require dynein, which is localized by the polarity domain for proper function.

Asymmetric Cell Division in Plants

Asymmetric stem cell divisions are similarly necessary for proper plant development. Like animals, plants rely on ACDs to maintain a population of stem cells and promote growth. Because plant cells are immobile due to their rigid cell walls, ACD orientation is particularly important to ensure proper daughter cell position during development, but the mechanisms controlling ACD orientation in plants remain mostly mysterious.

Many studies on ACD mechanisms have been performed in *Arabidopsis thaliana,* which is ideal as a model organism due to its rapid growth, compact size, prolific seed production, ability to self-pollinate, and ability to introduce genetic mutations while maintaining fertility.

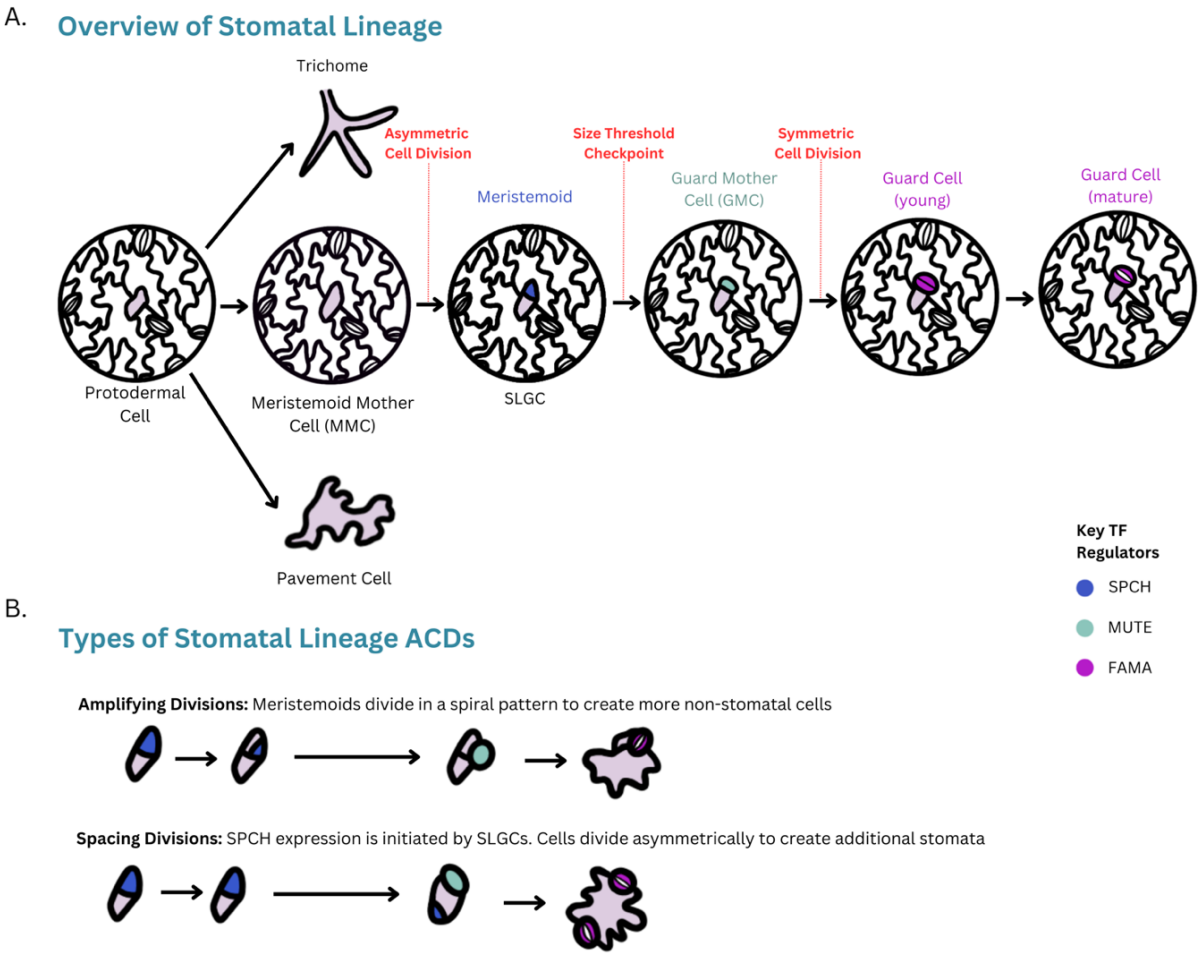

Figure 1: Overview of the Stomatal Lineage Pathway (Adapted from Lee & Bergmann 2019)
A. Representation of the stomatal lineage pathway, from protodermal cell to a mature guard cell (GC).
B. Types of stomatal lineage asymmetric cell divisions, utilized for proper spacing of stomata and for leaf patterning.

The Stomatal Lineage Patterns the Leaf Epidermis

Stomata are circular pores in plants that are created by pairs of guard cells. Stomata mediate gas exchange and water loss in plants during photosynthesis and transpiration, as the associated guard cells can adjust the size of the pore via changes in osmotic pressure (Araújo et al. 2011).

Stomata are generated and patterned through sequential asymmetric and symmetric cell divisions (Figure 1). Protodermal cells in the leaf epidermis can make branching differentiation decisions to become trichomes, pavement cells, or guard cells. The protodermal cells that enter this decision tree are considered to be in the stomatal lineage (Lee & Bergmann 2019).

Asymmetric cell divisions are key to establishing daughter cells of differing fates, placements, and sizes throughout the leaf epidermis. Each asymmetric division forms two daughter cells of differing sizes. The larger of the two daughter cells becomes a stomatal lineage ground cell (SLGC), whereas the smaller cell becomes a meristemoid. Through repeated rounds of ACDs, meristemoids perform amplifying divisions to increase the number of non-stomatal cells in the tissue. The SLGC can also perform an additional ACD, called a spacing division, that increases the relative stomatal number in the leaf (Lee & Bergmann 2019; Nadeau & Sack 2002; Robinson et al. 2011). During the spacing division, the resulting meristemoid will be positioned away from existing stomata to avoid the creation of adjacent stomata. Stomata are typically positioned around either undifferentiated cells or pavement cells, which are terminally differentiated epidermal cells that constitute most of the epidermis (Du & Jiao 2020). Therefore, ACD regulation is one of the foundations of the one-cell spacing rule (Hara et al. 2007), which states that there is at least one non-stomatal cell between each stomata. These amplifying and spacing divisions allow for stomatal distribution and density control.

The primary focus of this project is on the meristemoid mother cells (MMCs)/meristemoids and mature guard cells. In *Arabidopsis thaliana* meristemoids, cell size, and more specifically, the size of the nucleus, controls the timing of asymmetric cell

divisions. Meristemoids will perform self-renewing divisions until they receive a signal to commit to terminal differentiation (Figure 1). With each self-renewing division, the meristemoid, and thus its nucleus, decreases in size. When the nucleus crosses a critical size threshold, the process of asymmetric self-renewing divisions ceases and the cell commits to terminal differentiation by transitioning into a guard mother cell (GMC) (Gong et al. 2023).

Alongside the cellular components that control ACDs, several basic helix-loop-helix (bHLH) transcription factors act as key regulators of progression through the stomatal lineage. These bHLH transcription factors, SPEECHLESS (SPCH), MUTE, and FAMA, mediate the transition between different cell identities in the stomatal lineage pathway (Figure 1) (MacAlister et al. 2007, Pillitteri et al. 2007 and Ohashi-Ito & Bergmann 2006). SPCH regulates meristemoid fate by promoting asymmetric cell divisions, and meristemoids in *spch* mutants transition to pavement cells and never make stomata (MacAlister et al. 2007; Wallner et al. 2023).

Typically, division patterns in the epidermis of wild-type *Arabidopsis thaliana* are predictable depending on orientation of the protodermal cell to the tissue axis or cellular niche, plus the one-cell spacing rule. For example, meristemoids position their division planes so that new meristemoids are not directly adjacent to other meristemoids, guard mother cells (GMCs) or stomata (Hara et al. 2007). Any changes in stomatal density or overall phenotype (such as adjacent stomata) may indicate an alteration in the mechanism behind asymmetric cell division.

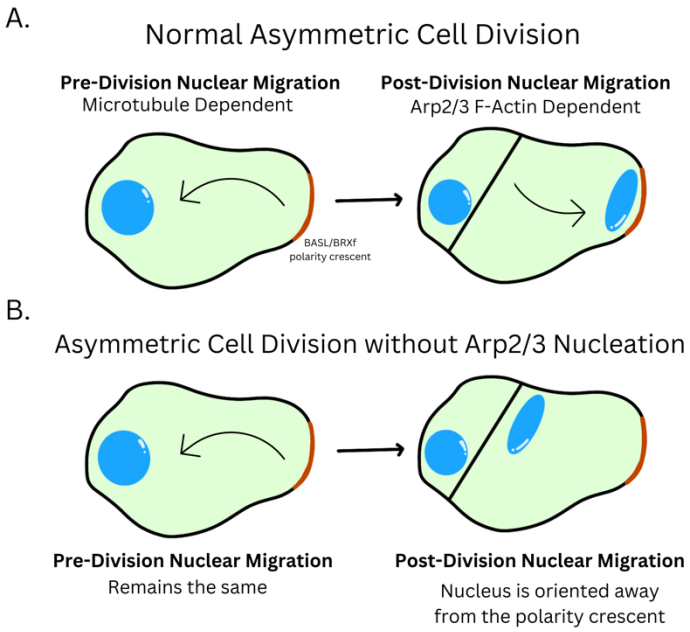

Figure 2: Nuclear Migration During Stomatal Lineage ACDs

A. Representation of wild-type nuclear migration in relation to the polarity crescent (data from Muroyama et al. 2020).

B. Representation of nuclear migration in the absence of Arp2/3 actin nucleation (data from this thesis).

Nuclear Migration Guides Asymmetric Cell Divisions

Asymmetric stem cell divisions are often guided by nuclear migration to properly position daughter cells and control the partitioning of cellular components. In the *Arabidopsis* zygote, F-actin mediates nuclear positioning during asymmetric cell division by forming a cap that guides the nucleus to the apical side of the zygote (Kimata et al. 2016). Asymmetric cell divisions in lateral roots initiation are carried out by a localized auxin response and involve directional nuclear migration (Goh et al. 2019). In both of these examples, however, the molecular regulators of nuclear movement remain unknown.

In the *Arabidopsis thaliana* stomatal lineage, asymmetric divisions utilize the plasma membrane-associated polarity complex proteins, BREAKING OF ASYMMETRY IN THE STOMATAL LINEAGE (BASL) and BREVIS RADIX family (BRXf) proteins, which form a polarity crescent before mitosis (Dong et al 2009). This BASL/BRXf polarity crescent

recruits POLAR, which enhances the activity of GLYCOGEN SYNTHASE KINASE3 (GSK3)-like kinases to promote ACDs (Pillitteri et al. 2011; Houbaert et al. 2018). Previous research shows that cortical BASL/BRXf is sufficient and necessary to guide nuclear migration throughout ACDs, leading to proper nuclear position pre- and post-division (Muroyama et al. 2020). In a typical asymmetric cell division, the nucleus is initially guided away from this polarized crescent before each ACD (NM^{pre}) by microtubules. This directly contrasts with the post-divisional orientation of the nucleus (NM^{post}), which re-positions the nucleus directly adjacent to the polarized crescent, approximately 8-10 hours post-division (Figure 2).

It is known that NM^{pre} is mediated by microtubules, whereas NM^{post} is mediated by F-actin and at least one myosin (Muroyama et al. 2020). This myosin, MYOXI-I, is in the Myosin XI family, a plant specific myosin family that is responsible for cytoplasmic streaming and the movement of organelles. It is associated with the nuclear envelope and mediates the spindle shape of nuclei in pavement cells (Kimata et al. 2016).

NM^{post} is required for proper stomatal patterning during leaf development. Because amplifying and spacing divisions in the wild-type position stomata to avoid stomatal clusters, stomata pairing or a change in stomatal density in mutant lines may indicate that the mutant gene plays a role in nuclear migration. Because MYOXI-I is known to mediate post-division nuclear migration it is expected that altered stomatal spacing has been noted in the *myoxi-i* mutant, which has a significantly lower stomatal density than the wild-type. This indicates that a change in stomatal density for a *myoxi-i* mutant also indicates that changes in nuclear migration can affect stomatal density (Muroyama et al. 2020).

While it has been shown that NM^{post} is dependent on F-actin (Muroyama et al. 2020), the types of F-actin arrays that control NM^{post} remain unknown.

Actin Microfilaments Aid in Cell Division

Actin is highly conserved and, along with tubulin, forms one of the major eukaryotic cytoskeletons. Actin exists in two forms within cells: F-actin and G-actin. G-actin, or globular actin, is the monomeric form of actin that polymerizes into linear F-actin filaments. F-actin, or filamentous actin, is dynamic and can undergo cycles of polymerization and depolymerization that are mediated by ATP hydrolysis (Lappalainen et al. 2022; Kudryashov & Reisler 2013). These dynamics are essential for many important cell functions, including cell division and organelle movement. (Gibieža & Petrikaitė 2021).

Nucleation of new F-actin filaments is the rate-limiting step in F-actin filament creation. To facilitate this process, cells have evolved means of promoting nucleation, including the evolution of two major classes of F-actin nucleators, the Arp2/3 complex and formins. The actin-related protein 2/3 (Arp2/3) complex is a large protein complex that is comprised of seven subunits: Arp2, Arp3, p40 (ArpC1), p34 (ArpC2), p21 (ArpC3), p20 (ArpC4), and p16 (ArpC5). It promotes the formation of branched F-actin networks by nucleating a new filament off the side of a pre-existing filament. This new filament forms at a 70° angle to the original actin filament to form a Y-shaped branch (Goley & Welch 2006; Roullier et al. 2008). The second form of actin polymerization is formin-mediated nucleation. Formins are a protein family that are known to create long, unbranched actin filaments. Formin-nucleated actin is also known to affect cell polarity (Breitsprecher & Goode 2013; Evangelista et al. 2002). Within the context of nuclear migration in the *Arabidopsis* stomatal

lineage, it is unknown if NM^{post} relies on Arp2/3-dependent actin nucleation or formin-mediated actin nucleation.

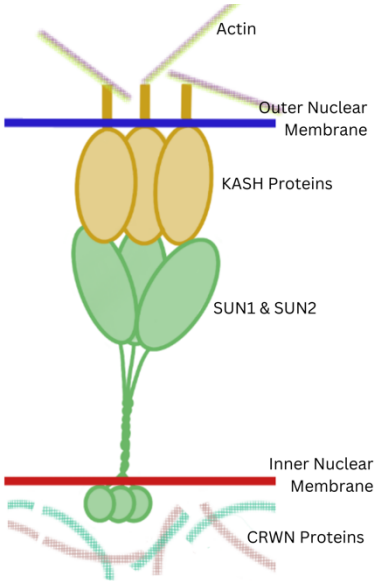

Figure 3: Localization for the SUN, KASH, and CRWN Proteins in the Nuclear Envelope
The SUN protein forms a nuclear envelope-spanning complex the KASH proteins to link the cytoskeleton and nucleoskeleton. The KASH protein links actin to the nuclear envelope. The CRWN protein is localized to the nuclear lamina and distributes chromatin.

Protein Candidates that Control Nuclear Morphology and Nucleus-Cytoskeleton Interactions

The proteins of interest for the project included CRWN1, CRWN3, SUN1, SUN2, and SINE1. These proteins were selected because of their known roles in mediating nuclear shape/size and interactions between the nucleus and F-actin cytoskeleton.

The CROWDED NUCLEI series of mutants, or *crwn*, are known to have nuclei with decreased size, altered shape, and perturbed heterochromatin orientation (Wang et al. 2013). The CRWN protein builds a meshwork structure via their localization at the nuclear lamina (Figure 3). Additionally, CRWNs manage the distribution of chromatin and gene expression

(Sakamoto et al. 2020). CRWN loss-of-function leads to a smaller nuclear size but unaltered overall cell size. This change is the most obvious in the *crwn1* mutant, although the nuclear DNA density may be up to four times higher than the wildtype in all *crwn* mutants (Wang et al. 2013). It is also known that meristemoids in *crwn1* (and likely all *crwn* mutants) commit to the stomatal lineage pathway earlier in development, compared to the wild-type. This is due to nuclear size acting as a regulator for stomatal differentiation (Gong et al. 2023).

The Sad1/UNC-84 (SUN) domain protein is a nuclear envelope protein that connects the cytoskeleton to the nucleoskeleton of the cell via the KASH protein (Figure 3). This then links telomeres to the cytoplasm. *sun1* and *sun2* mutants have elongated nuclei in epidermal cells. Both *sun1* and *sun2* also have a meiotic delay and other severe defects in meiosis, such as altered chiasma frequency, which are structures that link chromosomes together before anaphase I. Overall, these defects alter chromosome movement throughout mitosis. (Varas et al. 2015). However, their roles in regulating nuclear migration during ACD remain unexplored.

Finally, *sine1* has an altered KASH protein. The KASH protein is involved in F-actin binding at the nuclear envelope, connecting the nucleus to the cytoskeleton (Figure 3). Because previous literature indicates that F-actin mediates post-division nuclear migration, it is possible that a defect in the KASH protein may not allow F-actin to properly bind at the nuclear envelope and thus affect post-division nuclear migration (Muroyama et al. 2020; Biel et al. 2020).

While some of the roles of these proteins are known in other plant tissues, their effects on nuclear migration and asymmetric division are still unknown.

SALK Lines

To study gene function in *Arabidopsis*, many research groups utilize a collection of mutant lines, colloquially called "Salk lines." The Salk Institute created ~88,000 *Arabidopsis thaliana* lines with transfer DNA (T-DNA) insertions in order to disrupt gene function (Alonso et al. 2003). These lines are instrumental in researching *Arabidopsis* genes, as the knockout mutations created by T-DNA insertions simplify the process of determining gene function (Pucker 2021). Multiple SALK line *Arabidopsis thaliana* mutants have been identified as having different nucleus or nuclear envelope defects.

Because asymmetric cell division is responsible for the creation of stomata (Figure 1), these mutants can be used to determine if mutations in specific nuclear-envelope-localized proteins create defects in stomatal placement or density. Any changes in stomatal phenotype in the aforementioned mutant lines, compared to a wildtype, could indicate a possible link between the given gene and nuclear migration.

Goals of the Project

The overarching goal of this project is to determine the mechanism by which the nucleus is positioned during asymmetric cell divisions in the *Arabidopsis* stomatal lineage pathway. This will be accomplished by determining the molecular mechanism that *Arabidopsis thaliana* utilizes to regulate nuclear movement and by determining which genes are required for proper nuclear migration.

CHAPTER 2: MATERIALS & METHODS

A. Seed Sterilization & Growth

Seeds were sterilized in 20% bleach for 10 minutes and washed three times in sterile milliQ H_2O. They were then plated on 1/2 Murashige and Skoog (MS) plates with 0.5% sucrose. Plates were stratified in the dark at 4°C for at least 3 days and then grown vertically at 22°C under long day conditions (16 h light/8 h dark).

B. Propidium Iodide Staining

Propidium iodide (PI) (Thermo Fisher Scientific, #P3566) was used to dye cell walls, allowing them to be easily viewed with a microscope. Seedlings were incubated in a 1:100 dilution of PI for 30 minutes. The bottom left area of the abaxial side of each cotyledon, or embryonic leaf, was imaged in order to capture a consistent area to be analyzed for stomatal density. Images were captured with 20x magnification using laser 561 on the Leica Stellaris 5 microscope with HyD detectors. Each image captured an area of .268 mm^2.

C. Crossing

Healthy, unopened flower buds were chosen for crossing. Any siliques or open flowers/buds in the vicinity were removed. The petals and sepals were removed from the closed bud with forceps to reveal the stigma. An open flower from the other plant of interest was selected and gently dabbed on the uncovered stigma to transfer the pollen. Siliques were collected after 2 weeks for downstream processing/analysis.

D. Genotyping

To extract genomic DNA, plant tissue (seedling or dissected leaf) was added to a microcentrifuge tube with 60uL of 0.4 N NaOH and was ground using a pestle. Samples were then placed in a 60°C water bath for 1 minute and centrifuged at 15,000xg for 60 seconds.

1uL of the supernatant was added to 49μL of 0.1 M Tris-HCl (pH 8.0). For PCR analysis, a master mix was prepared using 2.0X Taq Red Master Mix, a left and right primer for each sample, and MilliQ water. 14 μL of this master mix is added to 1 μL of DNA. The PCR program includes a 5 minute hold at 95ºC, 35 cycles of 30 seconds at 95ºC, 30 seconds at 58ºC, 1 minute at 72ºC, and a final 5 minute extension at 72ºC. The genotyping result is then checked using gel electrophoresis.

Table 1: Primers Used for Genotyping Mutants and Crosses
Left and right primers, and their associated sequences for each tested genotype. Primers were used to test for either the presence of the wild-type (WT) sequence, or for the presence of a T-DNA insertion for each genotype.

Purpose	Left Primer + Sequence	Right Primer + Sequence
WT CRWN1 allele	ADM36 GCTTAGTGGGTGATGACTCAAC	ADM38 CCTTCTCTTTGTTAATTTCTG
Mutant CRWN1 allele	ADM1 ATTTTGCCGATTTCGGAAC	ADM19 AGTTTCCAATGCCTTCTCCTC
WT CRWN3 allele	ADM22 TTGCCTCTGAAATTCCATGTC	ADM23 CAGTGACGCATATACGCATTC
Mutant CRWN3 allele	ADM1 ATTTTGCCGATTTCGGAAC	ADM23 CAGTGACGCATATACGCATTC
WT SUN1 allele	ADM24 CTGATCAAGATTCGTTCCCAC	ADM25 TACCAGAGGCTTTCACATTGG
Mutant SUN1 allele	ADM1 ATTTTGCCGATTTCGGAAC	ADM25 TACCAGAGGCTTTCACATTGG
WT SUN2 allele	ADM26 GACCAAACATGGGTTGACTTG	ADM27 GGTCACACATTGCTTTCCATC
Mutant SUN2 allele	ADM1 ATTTTGCCGATTTCGGAAC	ADM27 GGTCACACATTGCTTTCCATC

E. Stomatal Density

crwn1 (SALK_025347), *crwn3* (SALK_099283), *sun1* (SALK_123093), *sun2* (SALK_049398), and *sine1* (SALK_018239) lines were acquired from Arabidopsis

Biological Resource Center. *crwn1 crwn2* and *sun1 sun2* crosses were generated using the protocol mentioned above. Each plate was divided in half to plate mutant lines on the same plates as the wild-type to account for any differences in growth conditions. Each single mutant was imaged in four separate experiments. Both double mutant crosses were imaged four times.

F. Microscopy

Leica Stellaris 5 confocal microscope with HyD detectors and a PL APO 20x 0.75 NA objective and LAS X software was utilized for all imaging.

G. Drug Treatment Dosage

To experimentally validate the dosage of the F-actin drugs used in this work, 3dpg UBQ10p::mCherry-ABD2-mCherry seedlings were incubated with 1 μM, 5 μM, 10 μM, and 20 μM CK-666 (Sigma-Aldrich, #182515-25MG), CK-689 as a negative control (Sigma-Aldrich, #182517-25MG), Latrunculin B as a positive control (Fisher-Scientific, 39-741), or DMSO as a negative control (Fisher Scientific, D128-500) for 5 hours. Drugs were diluted with 1/2 Murashige and Skoog (MS) with 0.5% sucrose to achieve each dosage. They were then imaged with identical laser and gain settings to examine the effects of drug treatment on F-actin levels and organization. Because images were acquired with consistent intensity settings, relative F-actin levels in each cell were evaluated.

H. Time Lapse Imaging

3dpg BRXL2p::BRXL2-YFP ML1p::mCherry-RCI2A ML1p::GFP-NLS seedlings were placed in a flow chamber (Hybriwell, HBW75). Wells were filled with 1/2 Murashige and Skoog (MS) with 0.5% sucrose containing 10 μM CK-666 or CK-689. Tubing was routed from a peristaltic pump (set to a rate of .4 mL/hr) to the flow chamber, to maintain a constant

flow of 10 μM treatment and 1/2 MS with 0.5% sucrose throughout the course of the time lapse. Because the time-lapse acquisition setup cannot be used to simultaneously image different treatment conditions, different treatments were carried out in different imaging sessions. Seedlings were imaged for a total of 15-20 hours, with images being taken every 30 minutes. ACDs were then identified and analyzed using FIJI software.

I. Image Analysis

All images were analyzed using FIJI software. For stomatal phenotyping, images of a constant size and region for all genotypes and controls were compared by creating a MAX projection and counting all visible, mature stomata. For drug treatment tests, the image brightness was kept uniform and MAX projections were used for comparison. For time lapse imaging, a MAX projection was created of the entire time lapse. Asymmetric cell divisions were manually identified throughout the time lapse. Once identified, the distance between the nearest edge of the nucleus to the nearest edge of the polarity crescent (as labeled by BRXL2-YFP) was measured using FIJI's line tool.

J. Statistical Analysis

All statistical analyses were done in GraphPad Prism. For all tests that compare two variables (stomatal analysis of single mutants and time lapse imaging), a Mann-Whitney test was performed. For the stomatal analysis of the double mutant crosses, a one-way ANOVA was used. Mean and sample standard deviation were also determined for each genotype or drug treatment.

CHAPTER 3: RESULTS

A. Stomatal Lineage Phenotyping

Five SALK line mutants were analyzed to determine if they exhibited any stomatal phenotypes that deviated significantly from the wild-type. We examined two well-described stomatal phenotypes that can result from ACD defects: adjacent (paired) stomata or a change in stomatal density. The analyzed mutants include *crwn1* (SALK_031094), *crwn3* (SALK_099283), *sun1* (SALK_123093), *sun2* (SALK_049398), and *sine1* (SALK_018239). All analyzed mutants have been associated with nuclear/nuclear envelope phenotypes and/or play important roles in linking the nuclear envelope to the cytoskeleton (Varas et al. 2015; Biel et al. 2020; Sakamoto et al. 2020; Wang et al. 2013). Because of the mutants' association with the nucleus or nuclear envelope, any change in stomatal phenotype may indicate a possible change in nuclear migration, due to the previously demonstrated importance of nuclear migration on stomatal patterning.

To analyze the mutants, 7 dpg seedlings were incubated in propidium iodide, which is a dye that stains cell walls in living plant tissue. A consistent area and location were imaged for each analyzed cotyledon to control for developmental timing, as it is known that cotyledons exhibit a developmental gradient along their proximodistal axis. Stomata were counted to determine the stomatal density for the imaged area. The difference in stomatal densities were then compared between the paired wild-type and mutant samples to determine any difference in stomatal density or phenotype, such as directly adjacent stomata (stomatal clustering).

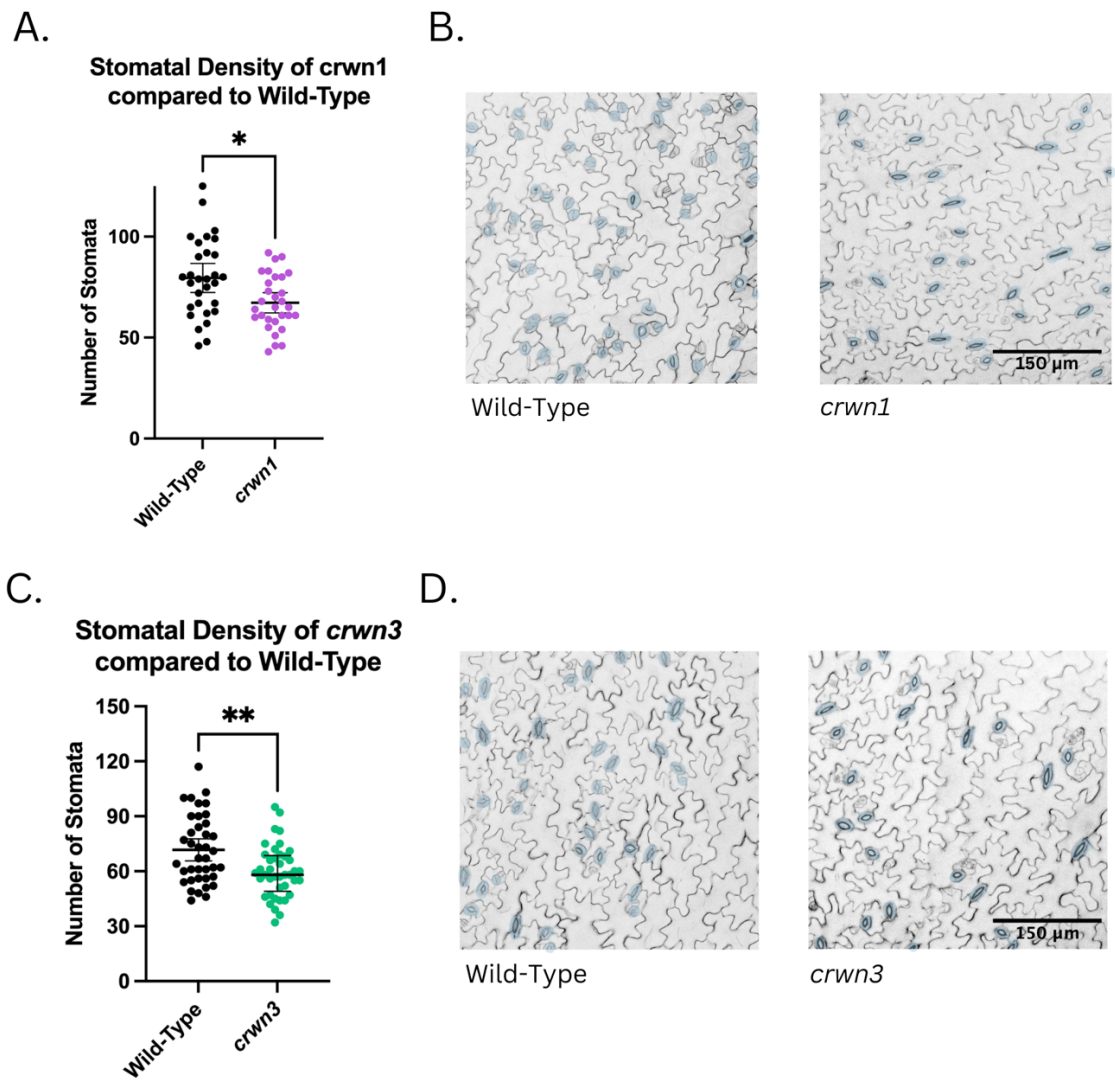

Figure 4: *crwn1* and *crwn3* decrease stomatal density

A. Stomatal density for *crwn1*, compared to the wildtype. Bars indicate the mean and 95% confidence interval. Significance is denoted with *, ns indicates no significant difference, as given by an unpaired t-test. n=31. 5 replicates were performed.

B. Images of 7 dpg wild-type and *crwn1* cotyledon phenotypes. Stomata are pseudo-colored blue.

C. Stomatal density for *crwn3*, compared to the wildtype. Bars indicate the mean and 95% confidence interval. Significance is denoted with *, ns indicates no significant difference, as given by an unpaired t-test. n=40. 5 replicates were performed.

D. Images of 7 dpg wild-type and *crwn3* cotyledon phenotypes. Stomata are pseudo-colored blue.

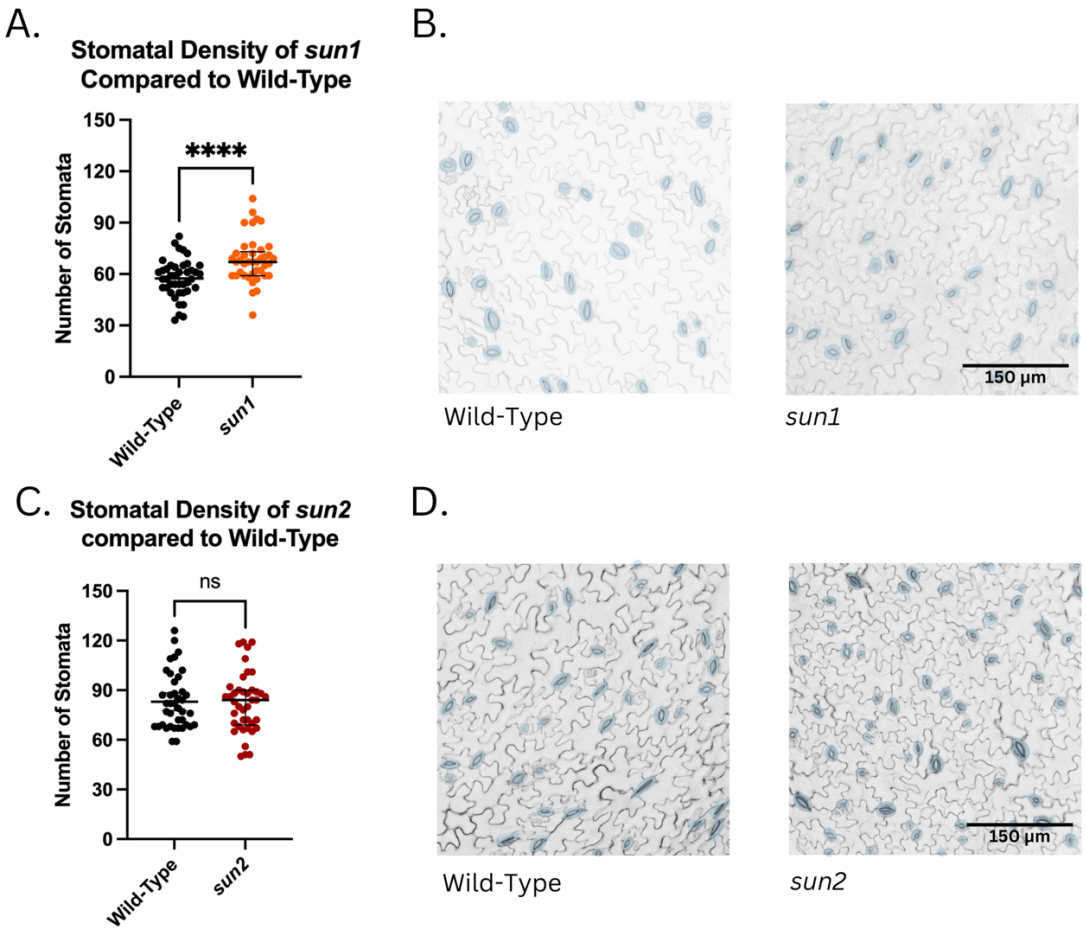

Figure 5: *sun1* increases stomatal density

A. Stomatal density for *sun1*, compared to the wildtype. Bars indicate the mean and 95% confidence interval. Significance is denoted with *, ns indicates no significant difference, as given by an unpaired t-test. n=41. 5 replicates were performed.
B. Images of 7 dpg wild-type and *sun1* cotyledon phenotypes. Stomata are pseudo-colored blue.
C. Stomatal density for *sun2*, compared to the wildtype. Bars indicate the mean and 95% confidence interval. Significance is denoted with *, ns indicates no significant difference, as given by an unpaired t-test. n=40. 5 replicates were performed.
D. Images of 7 dpg wild-type and *sun2* cotyledon phenotypes. Stomata are pseudo-colored blue.

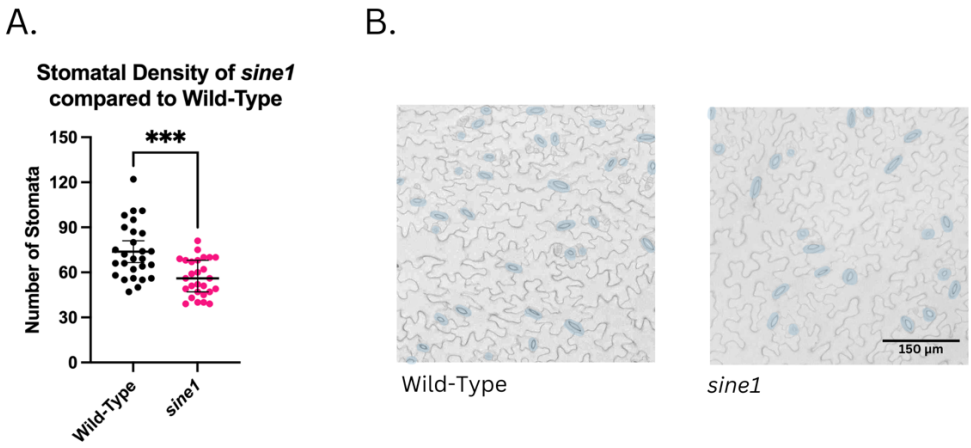

Figure 6: *sine1* decreases stomatal density
A. Stomatal density for *sine1*, compared to the wildtype. Bars indicate the mean and 95% confidence interval. Significance is denoted with *, ns indicates no significant difference, as given by an unpaired t-test. n=27. 5 replicates were performed for each genotype.
B. Images of 7 dpg wild-type and mutant cotyledon phenotypes. Stomata are pseudo-colored blue.

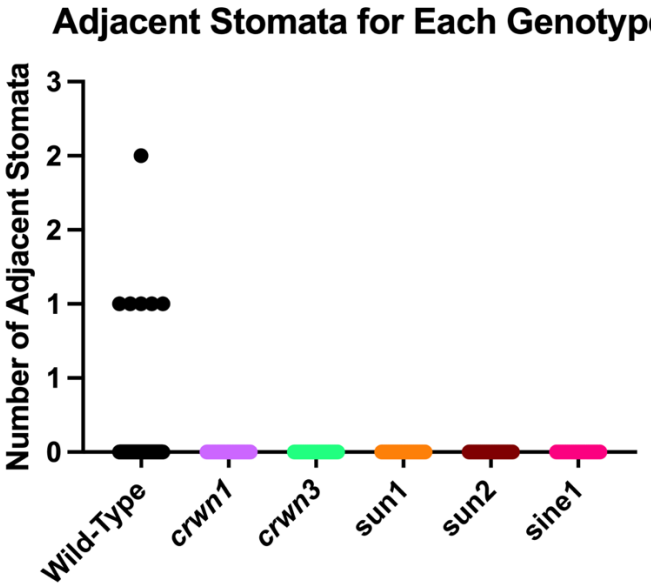

Figure 7: Mutant genotypes did not have significant adjacent stomata
Number of pairs of adjacent stomata for each analyzed sample and genotype. From left to right, n=179, n=31, n=40, n=41, n=40, n=27. 25 replicates were performed for the wild-type. 5 replicates were performed for each mutant genotype. No significant difference between the wild-type and mutants was present, as calculated by a one-way ANOVA.

Out of the five mutants that were analyzed, four had significant differences in stomatal patterning compared to the wild-type. These mutants, *crwn1, crwn3, sun1*, and *sine1*, each had altered stomatal density, but no apparent adjacent stomata. *crwn1, crwn3*, and *sine1* all had a decrease in stomatal density. *crwn1* had a stomatal density of 68±15, compared to the wild-type of 82±16. *crwn3* had a stomatal density of 56±14, compared to the wild-type of 70±16. *sine1* had a stomatal density of 56±12, compared to the wild-type of 73±19. *sun1* had an increase in stomatal density, at 69±17, up from 58±12 for the wild-type. Significance was determined with an unpaired T-test to compare the mutant to wildtype. Because the mutant and wild-type were plated on the same plate to control for growth conditions, mutants are compared to their respective wild-type. This accounts for any changes in wild-type stomatal density that could be due to differences in stratification time, plate batch, or other experimental variables.

B. Phenotyping for Redundancy Among Closely Related Genes

To determine whether genetic redundancy might be masking the effects on stomatal patterning, we generated double mutants lacking *crwn1 crwn3* and *sun1 sun2*. To identify and isolate homozygous double mutants, individual plants in the F2 generation from the crosses for *crwn1 crwn3* were genotyped using primers ADM36 and ADM38 to determine the presence of the wild-type CRWN1 allele, ADM1 and ADM19 to determine the presence of the mutant CRWN1 allele, ADM22 and ADM23 to determine the presence of the wild-type CRWN3 allele, and ADM1 and ADM23 to determine the presence of the mutant CRWN3 allele. Individual plants in the F2 generation for *sun1 sun2* were genotyped using primers ADM24 and ADM25 to determine the presence of the wild-type SUN1 allele, ADM1 and ADM25 to determine the presence of the mutant SUN1 allele, ADM26 and ADM27 to

determine the presence of the wild-type SUN2 allele, and ADM1 and ADM27 to determine the presence of the mutant SUN2 allele to identify and isolate homozygous double mutants. The resulting double mutants, *crwn1 crwn3* and *sun1 sun2*, were analyzed using the same PI phenotyping methods as previously mentioned to identify potential stomatal clustering or a change in stomatal density. When analyzing the double mutants, the respective single mutants were also included along with a Col-0 wild-type control to quantify whether any additive effects were seen. The *sun1 sun2* cross exhibited a higher stomatal density than the wild-type (76±14 for *sun1 sun2* compared to 57±11 for the wild-type), but it was not significantly different than sun1 (69±10). This indicates that SUN1 is the major driver of the stomatal phenotype. Only *crwn1 crwn3* (stomatal density of 48±10) exhibited a significant change from the stomatal density of both the wild-type (70±20) and the respective single mutants (70±15 for *crwn1* and 63±13 for *crwn3*. This indicates that *crwn1* and *crwn3* have overlapping functions.

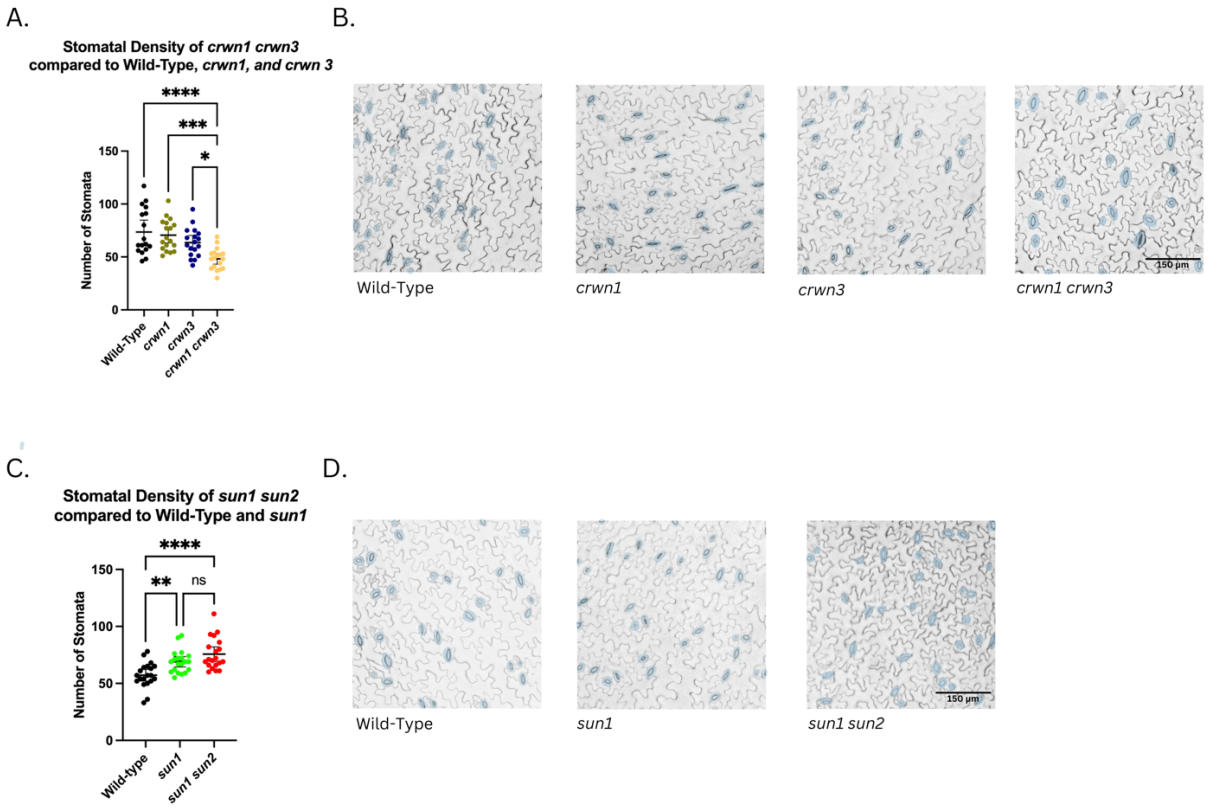

Figure 8: crwn mutation have overlapping function while sun1 is relevant homolog for stomatal patterning

A. Stomatal density for crosses, compared to the wildtype and single mutants. Bars indicate the mean and 95% confidence interval. Significance is denoted with *, ns indicates no significant difference, as given by a one-way ANOVA. n=20 with 4 replicates.

B. Images of 7 dpg wild-type and mutant cotyledon phenotypes. Stomata are pseudo-colored blue.

C. Stomatal density for crosses, compared to the wildtype and single mutants. Bars indicate the mean and 95% confidence interval. Significance is denoted with *, ns indicates no significant difference, as given by a one-way ANOVA. n=18 with 4 replicates.

D. Images of 7 dpg wild-type and mutant cotyledon phenotypes. Stomata are pseudo-colored blue.

C. Drug Treatment Dosage

To investigate the effects of Arp2/3 complex-mediated F-actin on post-ACD nuclear migration, it was necessary to identify the appropriate concentration and treatment length for the Arp2/3 complex inhibitor CK-666 (and associated inactive analog, CK-689) (Nolen et al. 2009; Hetrick et al. 2013). To determine an effective dose of the inhibitor, BRXL2p::BRXL2-

YFP TMM::mCherry-ABD2-mCherry 3dpg seedlings were incubated in varying doses of CK-666, CK-689 (negative control), DMSO (negative control), and Latrunculin B (positive control). This reporter line, generated in the Muroyama lab, expresses a 2 x mCherry-tagged version of the F-actin binding domain from fimbrin (ABD2) in early stomatal lineage cells via the TMM promoter. Based on what has been used previously in the literature, we tested concentrations of 1 μM, 5 μM, 10 μM, and 20 μM and assayed F-actin organization and seedling health (Liu et al. 2020; Xu et al. 2024). After a two-hour incubation period, seedlings were imaged using identical imaging conditions, including the same laser intensity and gain settings so that fluorescence intensity between different samples could be directly compared. Images for each drug and dose were then manually inspected to identify the concentrations that affected the total F-actin reporter signal and amount of branched F-actin.

Because Latrunculin B depolymerizes all F-actin, this acted as an important positive control for CK-666 to ensure only the branched Arp2/3 complex mediated F-actin was inhibited. As expected, the Latrunculin B showed almost no F-actin present in the cell, compared to the negative control of DMSO, which does not affect F-actin organization. None of the CK-666 dosages appeared to inhibit a similar level of F-actin, indicating that only Arp2/3 complex mediated F-actin was being inhibited.

Treatment with 1μM and 5μM CK-666 did not noticeably change either the levels of branched F-actin or reporter signal. In contrast, treatment with 20μM and 10μM of CK-666 showed a marked F-decrease in actin reporter signal and a decrease in branched F-actin structures. Because 20 μM and 10μM CK-666 showed similar effects in our assay, we opted to use the lower concentration, 10 μM, for subsequent time lapse imaging to maximize cell

viability and resource efficiency.

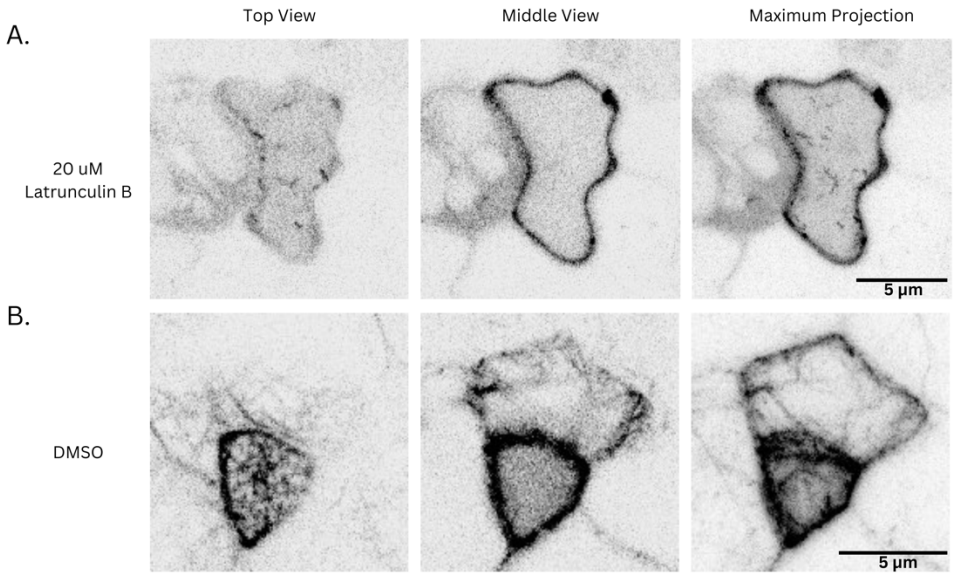

Figure 9: Latrunculin B effectively depolymerizes all F-actin
A. Cells incubated with 20 µM of Latrunculin B. Actin nucleation is indicated in black. Increased darkness and branching correspond to increased nucleation.
B. Cells incubated with DMSO. Actin nucleation is indicated in black. Increased darkness and branching correspond to increased nucleation.

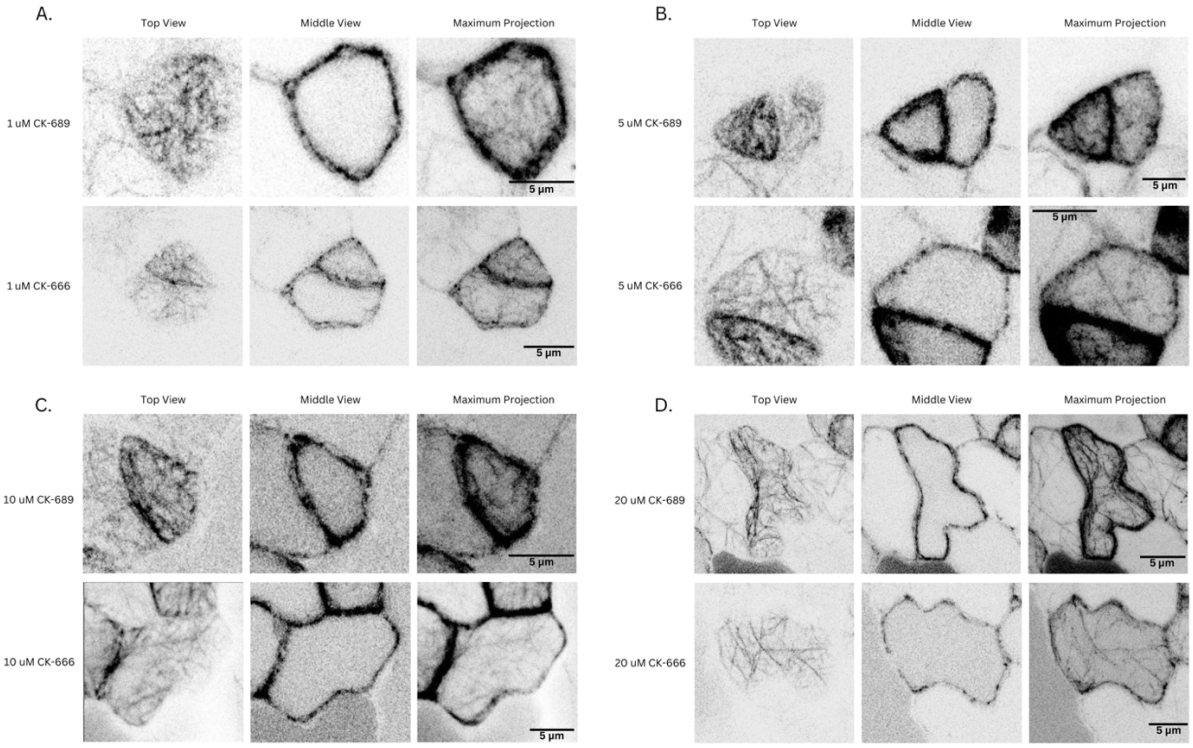

Figure 10: 10 and 20 µM of CK-666 effectively inhibit Arp2/3 complex
A. BRXL2p::BRXL2-YFP TMM::mCherry-ABD2-mCherry seedlings incubated with 1 µM of CK-666 compared to 1 µM CK-689. F-actin filaments are visualized in black. Increased darkness and branching correspond to increased nucleation.
B. BRXL2p::BRXL2-YFP TMM::mCherry-ABD2-mCherry seedlings incubated with 5 µM of CK-666 compared to 5 µM CK-689. F-actin filaments are visualized in black. Increased darkness and branching correspond to increased nucleation.
C. BRXL2p::BRXL2-YFP TMM::mCherry-ABD2-mCherry seedlings incubated with 10 µM of CK-666 compared to 10 µM CK-689. F-actin filaments are visualized in black. Increased darkness and branching correspond to increased nucleation.
D. BRXL2p::BRXL2-YFP TMM::mCherry-ABD2-mCherry seedlings incubated with 20 µM of CK-666 compared to 20 µM CK-689. F-actin filaments are visualized in black. Increased darkness and branching correspond to increased nucleation.

D. Post-division nuclear migration depends on Arp2/3-nucleated F-actin

Previous research showed that pre-division nuclear orientation (NM^{pre}) in the stomatal lineage is mediated by microtubules, which guide the nucleus away from the BASL/BRXL2 polarity crescent. After asymmetric cell division, the nucleus is guided towards the polarity

crescent in the SLGC (NM^{post}), which is mediated by F-actin (Muroyama et al. 2020). To determine whether the Arp2/3 complex controls nuclear positioning, 3dpg BRXL2p::BRXL2-YFP ML1p::mCherry-RCI2A ML1p::GFP-NLS *Arabidopsis thaliana* seedlings were incubated with either CK-666, an Arp2/3 inhibitor, or CK-689, an inactive analog that serves as the negative control. Pre-division nuclear migration is unaffected in both the treated and control cells, as expected, since it is not mediated by F-actin networks. Post-division migration was affected in the presence of CK-666, causing the nucleus to move away from the polarity crescent rather than towards it.

To quantify the behavior of the nucleus, we used FIJI to measure the distance from the outermost edge of the nucleus to the nearest point of the polarity crescent. Using this method, we found that the nucleus was 3.3+1.1 μm away from the polar domain 7-10 hours after division with CK-666 treatment compared to 0.8+0.7 μm in the CK-689 control. This result indicates that NM^{post} is mediated by Arp2/3 complex-nucleated F-actin.

A. Treatment with control drug (CK-689)

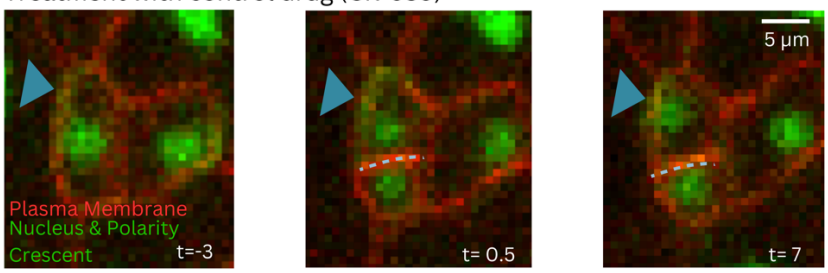

B. Treatment with Arp2/3 Inhibitor (CK-666)

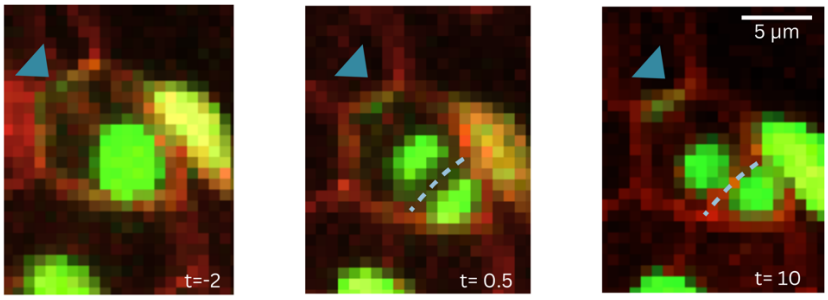

3dpg BRXL2p::BRXL2-YFP ML1p::mCherry-RCI2A ML1p::GFP-NLS seedlings

C.

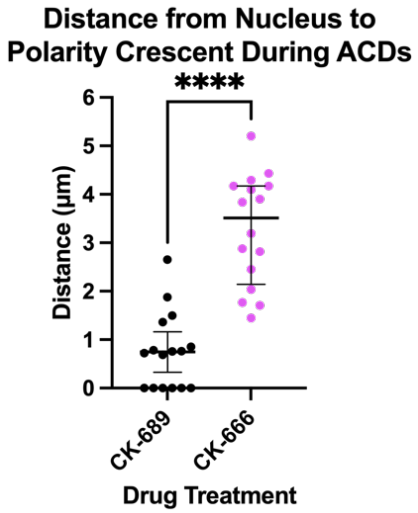

Figure 11: Nuclear Migration is Altered in Absence of Arp2/3 Complex-Nucleated F-Actin
A. 3dpg BRXL2p::BRXL2-YFP ML1p::mCherry-RCI2A ML1p::GFP-NLS cells incubated in CK-689, pre- and post-division. The polarity crescent is indicated with a blue arrowhead and new cell wall formation is indicated with a blue dashed line.
B. 3dpg BRXL2p::BRXL2-YFP ML1p::mCherry-RCI2A ML1p::GFP-NLS cells incubated in CK-666, pre- and post-division. The polarity crescent is indicated with a blue arrowhead and new cell wall formation is indicated with a blue dashed line.
C. Distance from the nucleus to the polarity crescent 7-10 hours post-division after treatment with either CK-689 or CK-666. n=16 with 4 replicates for each drug treatment. Significance is denoted with *, ****$p<0.0001$, ns indicates no significant difference as given by an unpaired t-test

CHAPTER 4: CONCLUSION

The purpose of this project was to identify new mediators of nuclear migration in asymmetrically dividing cells in the stomatal lineage. Based on a literature search, we tested whether five proteins with known roles in nuclear shape and nucleus-cytoskeleton interactions, CRWN1, CRWN3, SUN1, SUN2, and SINE1, are important for stomatal development. (Varas et al. 2015, Biel et al. 2020, Wang et al. 2013). Using stomatal phenotyping, we determined that four of these genes, *CRWN1, CRWN3, SUN1* and *SINE1*, impact stomatal density. As MYOXI-I, the only known mediator of post-division nuclear migration in the *Arabidopsis* stomatal lineage, also affects stomatal density, these new genes are ideal candidates for further exploration that could potentially control nuclear migration during ACDs. Additionally, previous research showed that post-division nuclear migration was mediated by F-actin (Muroyama et al. 2020). Through time-lapse imaging, we were able to determine that Arp2/3 complex-mediated F-actin nucleation mediates post-division nuclear migration.

While *sun1* did cause a significant stomatal phenotype, it notably had the opposite effect on stomatal density as the other mutants with stomatal phenotypes; stomatal density significantly increased in *sun1* while it decreased in the other mutants. As SUN1/SUN2 are thought to interact with KASH proteins (SINE1/2), it was unexpected that *sun1* and *sine1* would have opposite stomatal density phenotypes (Varas et al. 2015). Both involved proteins should link to form the nuclear envelope-spanning complex so we predicted that they would exhibit comparable phenotypes. Our results suggest that they may have previously unappreciated and separable functions, but more research is required to explore this question. Regardless, future studies into SUN1 are warranted as it alters amplifying and spacing

divisions in the stomatal lineage pathway. Alternatively, because the nuclear shape in *sun1* is altered, this may indicate that the change in nuclear shape alters nuclear migration or its ability to move as needed, rather than its effect on SUN/KASH interactions.

sine1 has an altered KASH protein, which is involved in F-actin binding in the nuclear envelope (Biel et al. 2020). Because previous research shows that F-actin is involved in NM^{post} (Muroyama et al. 2020), it is likely that the KASH protein does not allow F-actin to bind to the nuclear envelope properly, which would only alter post-division nuclear migration.

crwn1 and *crwn3* have a reduced nuclear size and altered spatial organization (Wang et al. 2013). Because nuclear migration heavily depends on the cell's spatial organization (especially regarding the nucleus and polarity crescent), this may explain the decrease in stomatal density for both mutants as the location of the nucleus is likely altered at all times, compared to the wild-type.

Due to the alterations in stomatal density, compared to the wild-type, it is possible that CRWN1, CRWN3, SUN1, and SINE1 proteins play a role in regulating nuclear migration. However, because we can only determine changes in cell fate via the final stomatal density, it remains possible that these changes are either due to a change in nuclear migration or another process associated with differentiation that remains to be identified. For example, *crwn1* is known to undergo additional rounds of asymmetric divisions before committing to the stomatal lineage pathway. This due to its reduced nuclear size, as the nucleus must reach a size threshold before the cell is triggered to terminally differentiate (Gong et al. 2023). Without further experimentation, we cannot definitively state that the reduced stomatal density is solely due to a change in nuclear migration.

To address this, in the future, fluorescent markers for the nucleus, plasma membrane, and polarity crescent could be introduced into the mutant backgrounds so that time-lapse imaging can be utilized to definitively test whether these loss-of-function mutants exhibit impaired nuclear migration.

In addition to analyzing changes in stomatal density of single mutants, we performed crosses to determine if genes within the same family exhibit any redundancy with each other. Due to time constraints, double homozygous mutants were screened using the stomatal density protocol. Because the stomatal phenotype for the *crwn1 crwn3* cross appeared to have an additive effect, compared to the single mutants, this indicates that the two genes have some overlapping function. The stomatal density of the *sun1 sun2* cross is not significantly different from the density of *sun1*, which was expected since *sun2* did not have a significant change in stomatal density, compared to the wild-type. This indicates that *SUN1* is the relevant homologue that contributes to stomatal development.

In addition to analyzing genetic factors behind nuclear migration, we also looked at the molecular mechanism of post-division nuclear migration. Comparing different doses of CK-666 (Arp2/3 complex actin inhibitor) to CK-689 (negative control for CK-689), Latrunculin B (actin inhibitor), and DMSO (negative control for Latrunculin B) using fluorescence microscopy to examine F-actin levels and organization revealed that 10 μM is the ideal dosage of CK-666 in order to maximize cell viability and resource efficiency over a 20 hour period, while having Arp2/3 complex actin nucleation effectively inhibited.

Using this dosage, we performed time-lapse imaging to determine how nuclear migration is affected with the inhibition of Arp2/3 F-actin nucleation. While Muroyama et al. (2020) previously uncovered that post-division nuclear migration is mediated via F-actin, the

type of F-actin was previously unknown. Because NM^{pre} is mediated through microtubule dynamics, whereas NM^{post} is mediated through actin dynamics, we specifically looked for a phenotype difference between CK-666 and CK-689 treatment, post-division. We measured the distance from the nucleus to the polarity complex 8 hours post-division, by which time the nucleus has moved adjacent to the polar domain in wild-type cells. In the negative control treated with 10 μM CK-689, nuclear migrations both pre- and post-division occurred normally, with NM^{pre} migrating away from the polarity crescent and NM^{post} migrating towards the polarity crescent. In the presence of the Arp2/3 nucleation inhibitor, CK-666, NM^{pre} was unaffected, while NM^{post} was oriented in the opposite direction, away from the polarity crescent. Because pre-division nuclear migration, which is known to be mediated by microtubules, remained the same in both the experimental and control, it can be concluded that any changes in NM^{post} movement are due to the change in Arp2/3 complex mediated actin nucleation.

In the future, the time lapse imaging with drug treatment protocol will also be repeated with inhibitors for different forms of actin nucleators, such as formin. This is necessary to conclude if any other forms of F-actin play a role in post-division nuclear migration or if Arp2/3 complex mediated F-actin alone is sufficient to control it.

Through this research, we are able to conclude that *CRWN1*, *CRWN3*, *SUN1*, and *SINE1* likely play a role in nuclear migration. In addition, Arp2/3 complex mediated F-actin mediates post-division nuclear migration. By better understanding the mechanisms that control nuclear migration, we are able to gain additional insight into how organelle positioning controls asymmetric cell divisions and stomatal development. Because the cellular pathways that control stem cell division are key to plant development, understanding the

mechanisms behind them allows us to better understand how ACDs are regulated in order to properly differentiate cells in plants.

ACKNOWLEDGEMENTS

I thank Akanksha Garhewal the generation of the BRXL2p::BRXL2-YFP TMM::mCherryABD2mCherry line.

I thank the Salk Institute Genomic Analysis Laboratory for providing the sequence-indexed Arabidopsis TDNA insertion mutants.

REFERENCES

Ali MF, Fatema U, Peng X, Hacker SW, Maruyama D, Sun MX, Kawashima T. ARP2/3-independent WAVE/SCAR pathway and class XI myosin control sperm nuclear migration in flowering plants. Proc Natl Acad Sci U S A. 2020 Dec 22;117(51):32757-32763. doi: 10.1073/pnas.2015550117. Epub 2020 Dec 7. PMID: 33288691; PMCID: PMC7768783.

Alonso JM, Stepanova AN, Leisse TJ, Kim CJ, Chen H, Shinn P, Stevenson DK, Zimmerman J, Barajas P, Cheuk R, Gadrinab C, Heller C, Jeske A, Koesema E, Meyers CC, Parker H, Prednis L, Ansari Y, Choy N, Deen H, Geralt M, Hazari N, Hom E, Karnes M, Mulholland C, Ndubaku R, Schmidt I, Guzman P, Aguilar-Henonin L, Schmid M, Weigel D, Carter DE, Marchand T, Risseeuw E, Brogden D, Zeko A, Crosby WL, Berry CC, Ecker JR. Genome-wide insertional mutagenesis of Arabidopsis thaliana. Science. 2003 Aug 1;301(5633):653-7. Doi: 10.1126/science.1086391. Erratum in: Science. 2003 Sep;301(5641):1849. PMID: 12893945.

Araújo WL, Fernie AR, Nunes-Nesi A. Control of stomatal aperture: a renaissance of the old guard. Plant Signal Behav. 2011 Sep;6(9):1305-11. Doi: 10.4161/psb.6.9.16425. PMID: 21847028; PMCID: PMC3258058.

Bergstralh DT, Dawney NS, St Johnston D. Spindle orientation: a question of complex positioning. Development. 2017 Apr 1;144(7):1137-1145. Doi: 10.1242/dev.140764. PMID: 28351864.

Biel A, Moser M, Meier I. Arabidopsis KASH Proteins SINE1 and SINE2 Are Involved in Microtubule Reorganization During ABA-Induced Stomatal Closure. Front Plant Sci. 2020 Nov 20;11:575573. Doi: 10.3389/fpls.2020.575573. PMID: 33324432; PMCID: PMC7722481.c.

Blanpain C, Horsley V, Fuchs E. Epithelial stem cells: turning over new leaves. Cell. 2007 Feb 9;128(3):445-58. Doi: 10.1016/j.cell.2007.01.014. PMID: 17289566; PMCID: PMC2408375.

Bouvrais H, Chesneau L, Le Cunff Y, Fairbrass D, Soler N, Pastezeur S, Pécot T, Kervrann C, Pécréaux J. The coordination of spindle-positioning forces during the asymmetric division of the Caenorhabditis elegans zygote. EMBO Rep. 2021 May 5;22(5):e50770. Doi: 10.15252/embr.202050770. Epub 2021 Apr 26. PMID: 33900015; PMCID: PMC8097383.

Chen W, Chen L, Zhang X, Yang N, Guo J, Wang M, Ji S, Zhao X, Yin P, Cai L, Xu J, Zhang L, Han Y, Xiao Y, Xu G, Wang Y, Wang S, Wu S, Yang F, Jackson D, Cheng J, Chen S, Sun C, Qin F, Tian F, Fernie AR, Li J, Yan J, Yang X. Convergent selection of a WD40 protein that enhances grain yield in maize and rice. Science. 2022 Mar 25;375(6587):eabg7985. Doi: 10.1126/science.abg7985. Epub 2022 Mar 25. PMID: 35324310.

Breitsprecher D, Goode BL. Formins at a glance. J Cell Sci. 2013 Jan 1;126(Pt 1):1-7. doi: 10.1242/jcs.107250. PMID: 23516326; PMCID: PMC3603506.

Dong J, MacAlister CA, Bergmann DC. BASL controls asymmetric cell division in Arabidopsis. Cell. 2009 Jun 26;137(7):1320-30. Doi: 10.1016/j.cell.2009.04.018. Epub 2009 Jun 11. PMID: 19523675; PMCID: PMC4105981.

Du F, Jiao Y. Mechanical control of plant morphogenesis: concepts and progress. Curr Opin Plant Biol. 2020 Oct;57:16-23. Doi: 10.1016/j.pbi.2020.05.008. Epub 2020 Jun 30. PMID: 32619966.

Evangelista M, Pruyne D, Amberg DC, Boone C, Bretscher A. Formins direct Arp2/3-independent actin filament assembly to polarize cell growth in yeast. Nat Cell Biol. 2002 Jan;4(1):32-41. Doi: 10.1038/ncb718. Corrected and republished in: Nat Cell Biol. 2002 Mar;4(3):260-9. Doi: 10.1038/ncb770. PMID: 11740490.

Gibieža P, Petrikaitė V. The regulation of actin dynamics during cell division and malignancy. Am J Cancer Res. 2021 Sep 15;11(9):4050-4069. PMID: 34659876; PMCID: PMC8493394.

Gillies TE, Cabernard C. Cell division orientation in animals. Curr Biol. 2011 Aug 9;21(15):R599-609. Doi: 10.1016/j.cub.2011.06.055. PMID: 21820628.

Goh T, Toyokura K, Yamaguchi N, Okamoto Y, Uehara T, Kaneko S, Takebayashi Y, Kasahara H, Ikeyama Y, Okushima Y, Nakajima K, Mimura T, Tasaka M, Fukaki H. Lateral root initiation requires the sequential induction of transcription factors LBD16 and PUCHI in Arabidopsis thaliana. New Phytol. 2019 Oct;224(2):749-760. Doi: 10.1111/nph.16065. Epub 2019 Aug 10. PMID: 31310684.

Goley ED, Welch MD. The ARP2/3 complex: an actin nucleator comes of age. Nat Rev Mol Cell Biol. 2006 Oct;7(10):713-26. doi: 10.1038/nrm2026. PMID: 16990851.

Gönczy P, Pichler S, Kirkham M, Hyman AA. Cytoplasmic dynein is required for distinct aspects of MTOC positioning, including centrosome separation, in the one cell stage Caenorhabditis elegans embryo. J Cell Biol. 1999 Oct 4;147(1):135-50. Doi: 10.1083/jcb.147.1.135. PMID: 10508861; PMCID: PMC2164971.

Gong Y, Dale R, Fung HF, Amador GO, Smit ME, Bergmann DC. A cell size threshold triggers commitment to stomatal fate in Arabidopsis. Sci Adv. 2023 Sep 22;9(38):eadf3497. Doi: 10.1126/sciadv.adf3497. Epub 2023 Sep 20. PMID: 37729402; PMCID: PMC10881030.

Hara K, Kajita R, Torii KU, Bergmann DC, Kakimoto T. The secretory peptide gene EPF1 enforces the stomatal one-cell-spacing rule. Genes Dev. 2007 Jul 15;21(14):1720-5. Doi: 10.1101/gad.1550707. PMID: 17639078; PMCID: PMC1920166.

Houbaert A, Zhang C, Tiwari M, Wang K, de Marcos Serrano A, Savatin DV, Urs MJ, Zhiponova MK, Gudesblat GE, Vanhoutte I, Eeckhout D, Boeren S, Karimi M, Betti

C, Jacobs T, Fenoll C, Mena M, de Vries S, De Jaeger G, Russinova E. POLAR-guided signalling complex assembly and localization drive asymmetric cell division. Nature. 2018 Nov;563(7732):574-578. Doi: 10.1038/s41586-018-0714-x. Epub 2018 Nov 14. PMID: 30429609.

Jan YN, Jan LY. Polarity in cell division: what frames thy fearful asymmetry? Cell. 2000 Mar 17;100(6):599-602. Doi: 10.1016/s0092-8674(00)80695-9. PMID: 10761924.

Jiang K, Feldman LJ. Regulation of root apical meristem development. Annu Rev Cell Dev Biol. 2005;21:485-509. Doi: 10.1146/annurev.cellbio.21.122303.114753. PMID: 16212504.

Kimata Y, Higaki T, Kawashima T, Kurihara D, Sato Y, Yamada T, Hasezawa S, Berger F, Higashiyama T, Ueda M. Cytoskeleton dynamics control the first asymmetric cell division in Arabidopsis zygote. Proc Natl Acad Sci U S A. 2016 Dec 6;113(49):14157-14162. Doi: 10.1073/pnas.1613979113. Epub 2016 Nov 22. PMID: 27911812; PMCID: PMC5150365.

Knoblich JA. Asymmetric cell division: recent developments and their implications for tumour biology. Nat Rev Mol Cell Biol. 2010 Dec;11(12):849-60. Doi: 10.1038/nrm3010. PMID: 21102610; PMCID: PMC3941022.

Kudryashov DS, Reisler E. ATP and ADP actin states. Biopolymers. 2013 Apr;99(4):245-56. Doi: 10.1002/bip.22155. PMID: 23348672; PMCID: PMC3670783.

Lappalainen P, Kotila T, Jégou A, Romet-Lemonne G. Biochemical and mechanical regulation of actin dynamics. Nat Rev Mol Cell Biol. 2022 Dec;23(12):836-852. doi: 10.1038/s41580-022-00508-4. Epub 2022 Aug 2. PMID: 35918536.

Laux T. The stem cell concept in plants: a matter of debate. Cell. 2003 May 2;113(3):281-3. Doi: 10.1016/s0092-8674(03)00312-x. PMID: 12732137.

Lee LR, Bergmann DC. The plant stomatal lineage at a glance. J Cell Sci. 2019 Apr 26;132(8):jcs228551. Doi: 10.1242/jcs.228551. PMID: 31028153; PMCID: PMC6503951.

Liu Y, Siles L, Lu X, Dean KC, Cuatrecasas M, Postigo A, Dean DC. Mitotic polarization of transcription factors during asymmetric division establishes fate of forming cancer cells. Nat Commun. 2018 Jun 21;9(1):2424. doi: 10.1038/s41467-018-04663-1. PMID: 29930325; PMCID: PMC6013470.

Liu Z, Zhou Y, Guo J, Li J, Tian Z, Zhu Z, Wang J, Wu R, Zhang B, Hu Y, Sun Y, Shangguan Y, Li W, Li T, Hu Y, Guo C, Rochaix JD, Miao Y, Sun X. Global Dynamic Molecular Profiling of Stomatal Lineage Cell Development by Single-Cell RNA Sequencing. Mol Plant. 2020 Aug 3;13(8):1178-1193. doi: 10.1016/j.molp.2020.06.010. Epub 2020 Jun 24. PMID: 32592820.

Lytle NK, Barber AG, Reya T. Stem cell fate in cancer growth, progression and therapy resistance. Nat Rev Cancer. 2018 Nov;18(11):669-680. doi: 10.1038/s41568-018-0056-x. PMID: 30228301; PMCID: PMC8388042.

MacAlister CA, Ohashi-Ito K, Bergmann DC. Transcription factor control of asymmetric cell divisions that establish the stomatal lineage. Nature. 2007 Feb 1;445(7127):537-40. doi: 10.1038/nature05491. Epub 2006 Dec 20. PMID: 17183265.

Muroyama A, Gong Y, Bergmann DC. Opposing, Polarity-Driven Nuclear Migrations Underpin Asymmetric Divisions to Pattern Arabidopsis Stomata. Curr Biol. 2020 Nov 16;30(22):4467-4475.e4. doi: 10.1016/j.cub.2020.08.100. Epub 2020 Sep 17. Erratum

Nadeau JA, Sack FD. Stomatal development in Arabidopsis. Arabidopsis Book. 2002;1:e0066. doi: 10.1199/tab.0066. Epub 2002 Sep 30. PMID: 22303215; PMCID: PMC3243354.

Nelson WJ. Adaptation of core mechanisms to generate cell polarity. Nature. 2003 Apr 17;422(6933):766-74. doi: 10.1038/nature01602. PMID: 12700771; PMCID: PMC3373010.

Neumüller RA, Knoblich JA. Dividing cellular asymmetry: asymmetric cell division and its implications for stem cells and cancer. Genes Dev. 2009 Dec 1;23(23):2675-99. doi: 10.1101/gad.1850809. PMID: 19952104; PMCID: PMC2788323.

Ohashi-Ito K, Bergmann DC. Arabidopsis FAMA controls the final proliferation/differentiation switch during stomatal development. Plant Cell. 2006 Oct;18(10):2493-505. doi: 10.1105/tpc.106.046136. PMID: 17088607; PMCID: PMC1626605.

Pardal R, Heidstra R. Root stem cell niche networks: it's complexed! Insights from Arabidopsis. J Exp Bot. 2021 Oct 13;72(19):6727-6738. doi: 10.1093/jxb/erab272. PMID: 34173817; PMCID: PMC8513229.

Pillitteri LJ, Peterson KM, Horst RJ, Torii KU. Molecular profiling of stomatal meristemoids reveals new component of asymmetric cell division and commonalities among stem cell populations in Arabidopsis. Plant Cell. 2011 Sep;23(9):3260-75. doi: 10.1105/tpc.111.088583. Epub 2011 Sep 30. PMID: 21963668; PMCID: PMC3203429.

Pillitteri LJ, Sloan DB, Bogenschutz NL, Torii KU. Termination of asymmetric cell division and differentiation of stomata. Nature. 2007 Feb 1;445(7127):501-5. doi: 10.1038/nature05467. Epub 2006 Dec 20. PMID: 17183267.

Poliwoda S, Noor N, Downs E, Schaaf A, Cantwell A, Ganti L, Kaye AD, Mosel LI, Carroll CB, Viswanath O, Urits I. Stem cells: a comprehensive review of origins and emerging clinical roles in medical practice. Orthop Rev (Pavia). 2022 Aug 25;14(3):37498. doi: 10.52965/001c.37498. PMID: 36034728; PMCID: PMC9404248.

Pucker B, Kleinbölting N, Weisshaar B. Large scale genomic rearrangements in selected Arabidopsis thaliana T-DNA lines are caused by T-DNA insertion mutagenesis. BMC Genomics. 2021 Aug 6;22(1):599. doi: 10.1186/s12864-021-07877-8. PMID: 34362298; PMCID: PMC8348815.

Robinson S, Barbier de Reuille P, Chan J, Bergmann D, Prusinkiewicz P, Coen E. Generation of spatial patterns through cell polarity switching. Science. 2011 Sep 9;333(6048):1436-40. doi: 10.1126/science.1202185. PMID: 21903812; PMCID: PMC3383840.

Rouiller I, Xu XP, Amann KJ, Egile C, Nickell S, Nicastro D, Li R, Pollard TD, Volkmann N, Hanein D. The structural basis of actin filament branching by the Arp2/3 complex. J Cell Biol. 2008 Mar 10;180(5):887-95. doi: 10.1083/jcb.200709092. Epub 2008 Mar 3. PMID: 18316411; PMCID: PMC2265399.

Sakamoto Y, Sato M, Sato Y, Harada A, Suzuki T, Goto C, Tamura K, Toyooka K, Kimura H, Ohkawa Y, Hara-Nishimura I, Takagi S, Matsunaga S. Subnuclear gene positioning through lamina association affects copper tolerance. Nat Commun. 2020 Nov 20;11(1):5914. doi: 10.1038/s41467-020-19621-z. PMID: 33219233; PMCID: PMC7679404.

Smit ME, Vatén A, Mair A, Northover CAM, Bergmann DC. Extensive embryonic patterning without cellular differentiation primes the plant epidermis for efficient post-embryonic stomatal activities. Dev Cell. 2023 Mar 27;58(6):506-521.e5. doi: 10.1016/j.devcel.2023.02.014. Epub 2023 Mar 16. PMID: 36931268.

Tame MA, Raaijmakers JA, van den Broek B, Lindqvist A, Jalink K, Medema RH. Astral microtubules control redistribution of dynein at the cell cortex to facilitate spindle positioning. Cell Cycle. 2014;13(7):1162-70. doi: 10.4161/cc.28031. Epub 2014 Feb 10. PMID: 24553118; PMCID: PMC4013166.

Varas J, Graumann K, Osman K, Pradillo M, Evans DE, Santos JL, Armstrong SJ. Absence of SUN1 and SUN2 proteins in Arabidopsis thaliana leads to a delay in meiotic progression and defects in synapsis and recombination. Plant J. 2015 Jan;81(2):329-46. doi: 10.1111/tpj.12730. PMID: 25412930.

Volarevic V, Ljujic B, Stojkovic P, Lukic A, Arsenijevic N, Stojkovic M. Human stem cell research and regenerative medicine--present and future. Br Med Bull. 2011;99:155-68. doi: 10.1093/bmb/ldr027. Epub 2011 Jun 13. PMID: 21669982.

Wallner ES, Dolan L, Bergmann DC. Arabidopsis stomatal lineage cells establish bipolarity and segregate differential signaling capacity to regulate stem cell potential. Dev Cell. 2023 Sep 25;58(18):1643-1656.e5. doi: 10.1016/j.devcel.2023.07.024. Epub 2023 Aug 21. PMID: 37607546.

Wang H, Dittmer TA, Richards EJ. Arabidopsis CROWDED NUCLEI (CRWN) proteins are required for nuclear size control and heterochromatin organization. BMC Plant Biol.

2013 Dec 5;13:200. doi: 10.1186/1471-2229-13-200. PMID: 24308514; PMCID: PMC3922879.

Xu L, Cao L, Li J, Staiger CJ. Cooperative actin filament nucleation by the Arp2/3 complex and formins maintains the homeostatic cortical array in Arabidopsis epidermal cells. Plant Cell. 2024 Feb 26;36(3):764-789. doi: 10.1093/plcell/koad301. PMID: 38057163; PMCID: PMC10896301.

Zhou W, Lozano-Torres JL, Blilou I, Zhang X, Zhai Q, Smant G, Li C, Scheres B. A Jasmonate Signaling Network Activates Root Stem Cells and Promotes Regeneration. Cell. 2019 May 2;177(4):942-956.e14. doi: 10.1016/j.cell.2019.03.006. Epub 2019 Apr 4. PMID: 30955889.